1989

A Thermal Analysis of a Spirally Wound Battery Using a Simple Mathematical Model

T. I. Evans
Texas A & M University - College Station

Ralph E. White
University of South Carolina - Columbia, white@cec.sc.edu

Publication Info

Journal of the Electrochemical Society, 1989, pages 2145-2152.

A Thermal Analysis of a Spirally Wound Battery Using a Simple Mathematical Model

T. I. Evans* and R. E. White**

Department of Chemical Engineering, Texas A&M University, College Station, Texas 77843

ABSTRACT

A two-dimensional thermal model for spirally wound batteries has been developed. The governing equation of the model is the energy balance. Convective and insulated boundary conditions are used, and the equations are solved using a finite element code called TOPAZ2D. The finite element mesh is generated using a preprocessor to TOPAZ2D called MAZE. The model is used to estimate temperature profiles within a spirally wound D-size cell. The model is applied to the lithium/thionyl chloride cell because of the thermal management problems that this cell exhibits. Simplified one-dimensional models are presented that can be used to predict best and worst temperature profiles. The two-dimensional model is used to predict the regions of maximum temperature within the spirally wound cell. Normal discharge as well as thermal runaway conditions are investigated.

Many battery systems produce heat as they are discharged due to the exothermic nature of the electrochemical reactions occurring. This buildup of heat can result in dangerous conditions depending upon the cell design and physical system. Often, thermal modeling of these battery systems is accomplished by assuming that the different components of the battery interior can be represented by a homogeneous region (*i.e.*, core region) having average properties. This approach is useful because it greatly simplifies the analysis; however, it may not provide adequate results when the different components of the battery have vastly different thermal properties. Often the material used for separating the anode from the cathode has a much lower thermal conductivity than the electrodes themselves. This condition may lead to heat management problems in spirally wound designs when the heat flow is primarily in the radial direction. Heat management could be improved in the spiral design if heat flow can proceed out the spiral along the more conductive materials; however, the spiral path offers a much greater distance to traverse as opposed to the more direct radial path. This work shows that conduction of heat out the spiral, during normal operation, reduces cell temperatures but does not substantially reduce the temperature drop, the difference between the maximum and minimum cell temperatures, in the cell. However, when hot spots are present in the cell, conduction out the spiral is substantial and the temperature drop in the cell is reduced significantly.

The $Li/SOCl_2$ cell is an example of a spirally wound D-size cell that has a thermal management problem. It is an attractive primary energy source because of its high energy density (1, 2). However, researchers have observed that high discharge rates and high temperatures promote thermal runaway in these cells (1-5). Venting of toxic gases and explosions, due to the rapid pressure buildup at higher temperatures, have been reported (1-5).

The purpose of this paper is to present a model that can be used to predict temperature profiles, in time and two spatial dimensions, within a spirally wound D-size $Li/SOCl_2$ cell and to estimate the ability of this design to conduct heat out of the cell. One-dimensional approximations to the two-dimensional analysis will be investigated for comparison purposes. Predictions from a one-dimensional model for a C-size cell are compared with experimental data (6) to learn more about the thermal behavior of $Li/SOCl_2$ cells. Finally, hypothetical thermal runaway situations are simulated using the two-dimensional model and a one-dimensional approximation in order to determine if the spiral design offers any thermal advantage under such conditions.

Description of a spirally wound electrochemical cell.—Figures 1 and 2 show two different views of a spirally wound electrochemical cell. The cell is constructed by inserting the cell roll into a cylindrical can as shown in Fig. 1. Electrolyte is poured into the can and fills the porous regions of the roll so that a reservoir of electrolyte remains at the top of the roll. Electrodes are constructed by impregnating the electrode materials on both sides of the current collector mesh (usually a nickel mesh in the $Li/SOCl_2$ cell). The anode current collector is usually spot welded to the side of the can and tabs connected to the cathode current collector are welded to the center post protruding through the can lid. The cell roll is constructed by stacking the anode, separator, and cathode on top of each other and then rolling up the stack. A top view of the roll is shown in Fig. 2, which is the two-dimensional plane of interest. The current collectors, embedded in the middle of each electrode, are not shown in Fig. 1 or 2.

Description of a $Li/SOCl_2$ cell.—In a typical $Li/SOCl_2$ cell, the anode is lithium, the cathode is a porous carbon structure, and the separator is a glass matting material. The electrolyte consists of lithium tetrachloroaluminate ($LiAlCl_4$) in thionyl chloride ($SOCl_2$). During discharge, Li is oxidized

$$Li \rightarrow Li^+ + e^- \qquad [1]$$

and $SOCl_2$ is reduced

$$2SOCl_2 + 4e^- \rightarrow 4Cl^- + SO_2 + S \qquad [2]$$

The $SOCl_2$ is the active material at the cathode; the porous carbon structure provides the sites upon which the $SOCl_2$ is reduced. This redox couple generates heat as the cell is discharged and this heat must be conducted away at a fast enough rate so that unsafe conditions will not develop.

This brief description is a simple analysis of the actual physical system. It has been observed that the $Li/SOCl_2$ cell is a complex chemical and electrochemical system involving an unknown number of reactions (2). Szpak and Venkatasetty (7) state that modeling the $Li/SOCl_2$ cell is difficult due to the complexity of this physical system. They observe that as the cell discharges, the temperature and pressure of the cell change, the volume of electrolyte decreases, the electrolyte composition varies, and new phases appear. However, much can be learned by modeling a simplified picture of the actual system.

Previous models.—Previous workers (8, 9) have presented thermal models for battery systems. Bernardi *et al.* (8) give an excellent development of a general energy balance for electrochemical systems. They present a complete energy balance that requires the knowledge of concentration profiles and current fractions within the cell. However, the energy balance is formulated by assuming that the temperature of the battery is uniform and changes only with time. That is, flat temperature profiles are assumed *a priori*. Lee *et al.* (9) present a three-dimensional model for battery systems involving a number of batteries in one unit. However, they treat the interior region of each bat-

*Electrochemical Society Student Member.
**Electrochemical Society Active Member.

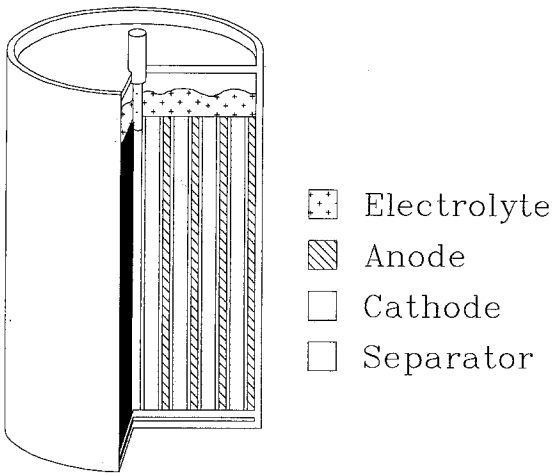

Fig. 1. Schematic representation of a spirally wound battery

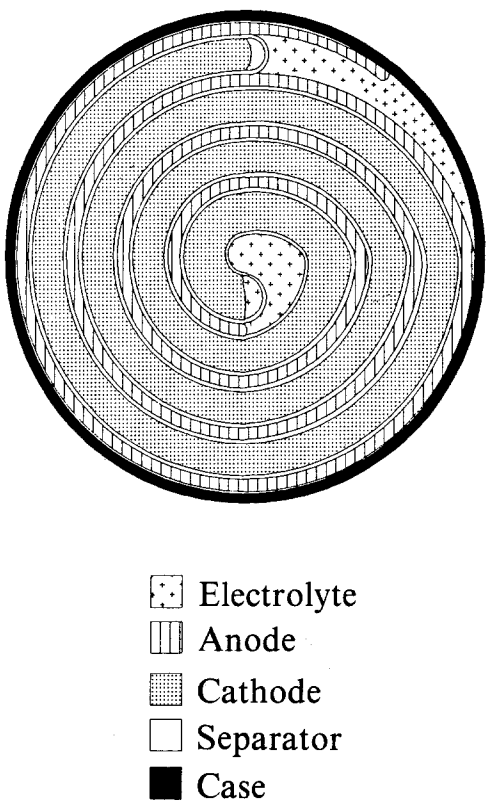

Fig. 2. Top view of a spirally wound battery

tery as a homogeneous phase having effective average properties. Therefore, the model cannot be used to predict the effects of the arrangement of the cell components on the temperature distribution.

Several models (10-19) have been presented which specifically address the thermal behavior of $Li/SOCl_2$ cells. Parnell and Szpak (10) present a thermal model for thin, disk-shaped $Li/SOCl_2$ cells in one dimension. They consider heat generation due to the polarization of the electrodes and internal cell resistance. A differential energy balance, which includes various terms representing different contributions to the heat generation, is solved numerically to obtain temperature profiles within the cell. Their model is used to show that as the rate of discharge is increased, the temperature increase is proportional to the increase in cell current. Szpak *et al.* (11) present a one-dimensional thermal model for disk-shaped $Li/SOCl_2$ cells, similar to the model by Parnell and Szpak (10), which accounts for catastrophic thermal runaway. This model is formulated by associating thermal runaway with ignition and burning, via one or more cell defects, rather than explosion. A differential energy balance and a differential material balance, which includes diffusion of species only, are solved simultaneously using a numerical method. The model is used to predict the time- and position-dependent temperature and concentration profiles. The model predictions compare favorably to what is physically observed, which may indicate that the reactions causing thermal runaway are initiated by localized heat sources developed from defective cells or cell components. Cho and Halpert (12) have presented a simple thermal model for spirally wound $Li/SOCl_2$ primary cells. In this work, an energy balance which requires an experimentally determined term for the heat generation rate is solved analytically to obtain the temperature of the cell as a function of time. They assume a uniform cell temperature which changes with time, as has been done by a number of workers (8, 13-16). Cho and Halpert (18) and Cho (19) have taken the modeling one step further by developing a means of calculating the heat generation rate term in their model (12) using experimentally determined resistances. An electrical circuit analogue is used that consists of the thermal resistances of the various cell components. None of these models can be used here, because each model treats the cell interior as one, pseudohomogenous material.

Other $Li/SOCl_2$ cell models have been developed (13-17). Evans *et al.* (13) and Tsaur and Pollard (14-17) use conservation of mass and charge to determine the concentration and reaction rate profiles in the cell. Both use porous electrode theory (20, 21) and concentrated solution theory (22-24) to develop the governing equations in one dimension. Evans *et al.* (13) include four cell regions in their model, whereas Tsaur and Pollard (14) essentially treat three cell regions. The boundary conditions used in each model are different and are based on different simplifying assumptions. It is assumed in each model that the cell temperature is uniform at any given moment in time. The cell temperature change with time is predicted using an overall energy balance. Tsaur and Pollard (15, 16) extend their model to include the additional species present when an acid electrolyte is utilized, such as in reserve cells (25). However, these previous models cannot be used to investigate the two-dimensional temperature profiles in spirally wound $Li/SOCl_2$ cells.

Model Formulation

The differential energy balance for region k of a battery can be written as

$$\rho_k c_{p,k} \frac{\partial T}{\partial t} = \nabla \cdot (\lambda_k \nabla T) + \sum_j \dot{q}'''_j \quad (j = 1, 2, \ldots) \qquad [3]$$

where $c_{p,k}$ and λ_k are the heat capacity and thermal conductivity of region k, respectively. In some instances, the steady-state temperature profiles are of interest, in which case the term $\partial T/\partial t$ in Eq. [3] is set to zero. The $\dot{q}'''_j$ terms in Eq. [3] represent various heat sources and sinks. Heat generated by polarization ($\dot{q}'''_p$) and heat generated due to the entropy change of the current producing reactions ($\dot{q}'''_s$), reactions 1 and 2, will be included in Eq. [3] for normal discharge conditions. The heat generation terms $\dot{q}'''_p$ and $\dot{q}'''_s$ are calculated as follows (26, 27)

$$\dot{q}'''_p + \dot{q}'''_s = \frac{\dot{q}_p + \dot{q}_s}{V_{cell}} \qquad [4]$$

where

$$\dot{q}_p + \dot{q}_s = I\left(E_{oc} - E - T\frac{dE_{oc}}{dT}\right) = I(E_{tn} - E) \qquad [5]$$

E_{tn} in Eq. [5], termed the thermoneutral potential, is the theoretical open-circuit potential of the cell at absolute zero. The cell voltage, E in Eq. [5], must be specified and can be obtained from experiment or predicted using an earlier model (13). Other sources/sinks of heat would include exothermic or endothermic chemical reactions occurring in the cell which do not produce current (27).

These sources are assumed to be negligible in this paper as is usually done for normal operation. To simulate thermal runaway, an additional $\dot{q}'''_j$ term is included in Eq. [3], $\dot{q}'''_d$, representing additional heating caused by, perhaps, a cell defect and/or exothermic chemical reactions. This heat source is assumed to be localized causing a hot spot in the cell. This approach to simulating thermal runaway was used by Szpak *et al.* (11).

To complete the mathematical description of the cell, the boundary conditions must be specified. For the cases investigated here, either a zero flux (insulated) boundary condition

$$\lambda_{k,x}\frac{\partial T}{\partial x}n_x + \lambda_{k,y}\frac{\partial T}{\partial y}n_y = 0 \qquad [6]$$

or a convection boundary condition

$$-\lambda_{k,x}\frac{\partial T}{\partial y}n_x - \lambda_{k,y}\frac{\partial T}{\partial y}n_y = h(T_w - T_A) \qquad [7]$$

is used. In Eq. [7], T_w is the temperature of the cell at its outer wall and is a function of x, y, and t, T_A is the surrounding temperature and is a fixed value, and h is a heat transfer coefficient. It is assumed here, for simplicity, that h is a constant and adequately characterizes the heat transfer through the cell casing and from the case wall to the surroundings via convection.

Solution Procedure

The finite element method (28, 29) is used to solve numerically Eq. [3], with Eq. [6] and [7], for the model region shown in Fig. 3. The computer package called TOPAZ2D (29) is used. Input files to TOPAZ2D, containing the coordinates of the finite element mesh, are created using another computer program called MAZE (30).

In order to obtain reliable, consistent results using the finite element method, a smooth mesh must be constructed and nodal points at region interfaces must match up. To achieve this, the two-dimensional spiral mesh is developed by constructing two semicircular meshes, offsetting one semicircular mesh, and then joining the two meshes together. Each semicircular mesh looks like half of a pie with many radial slices cut in it, as well as many concentric semicircles. A schematic of a model region constructed in this way is shown in Fig. 3, where **x** and **y** are the orthogonal vectors defining the two-dimensional plane and which intersect at the origin. The finite element mesh is not shown in Fig. 3 for clarity because it is fairly dense.

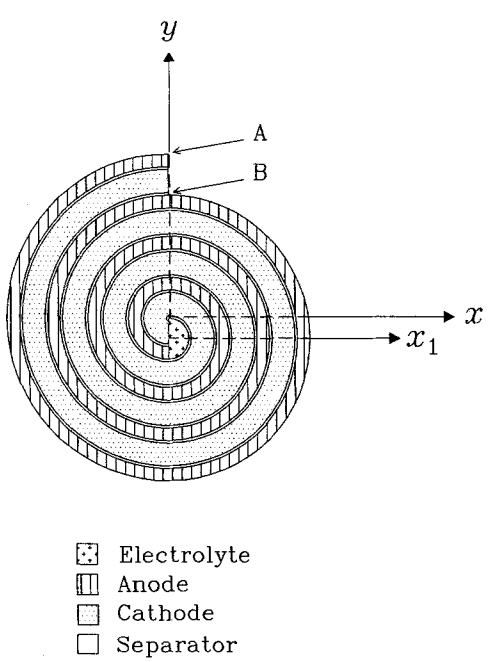

Fig. 3. The two-dimensional model region for the spiral design

To achieve the desired accuracy, between approximately 1000 and 8000 nodal points were used, depending on the particular problem to be solved. The vector $\mathbf{x}_1$ is shown in Fig. 3, because a temperature profile along this vector is shown later in this paper. The left half consists of four concentric semicircular cells and the right half consists of three concentric semicircular cells. Comparison of Fig. 2 and Fig. 3 shows that this construction provides a reasonable representation of the spiral design. For normal discharge conditions, meshes were refined until three-digit accuracy was obtained.

Table I lists the cell specifications for the spirally wound design investigated here. A similar cell is currently being developed by Wilson-Greatbatch (31) and may be used for applications in space (32). The thermophysical properties of each cell region and other model inputs are listed in Table II. Note that the properties for the cathode region and separator region are average properties calculated by assuming that all voids are filled with electrolyte. Here, the porous cathode was assumed to be 85% porous and the separator 70% porous.

Results and Discussion

Two simplified cases of the spiral design were investigated. The spiral was approximated using concentric circular regions, the top schematic in Fig. 4, and a core region, the bottom schematic in Fig. 4. The core region approach is based on the assumption that the cell interior can be represented by one homogeneous region. This core region possesses thermophysical properties which are the average of the properties of all the cell components. The core region properties were calculated as follows

$$\bar{p} = \frac{\Sigma_i \delta_i p_i}{\Sigma_i \delta_i} \qquad [8]$$

where δ_i is the thickness of region i and p_i is the value of a thermophysical property of region i as listed in Table II. The core properties are listed in Table II. These two cases simplify the calculations, because the governing equations need be solved in one dimension only. In fact, the steady-

Table I. Cell specifications for a spirally wound Li/$SOCl_2$ cell

Cell specification	Value	References
Thickness of cathode	1.12 mm	31, 38
Porosity of cathode	0.85	10, 38
Thickness of anode	0.7 mm	31, 32, 38
Thickness of current collector	0.14 mm	31, 32, 38
Thickness of separator	0.14 mm	31, 32, 38
Porosity of separator	0.7	38
Number of wraps	≈ 3 1/2	31, 32
D-size cell volume	≈ 4.94×10^4 mm^3	31, 32

Table II. Model inputs

	Thermophysical properties			
Material	Density (kg/m^3)	Thermal conductivity (W/m-K)	Specific heat (J/kg-K)	References
Lithium anode	534.0	71.1	3490.0	10, 11, 39
Nickel current collector	8900.0	90.5	444.0	11, 19
Carbon	1950.0	23.8	712.0	10, 11
Glass matting	220.0	0.242	963.0	10, 11, 38
Electrolyte (1.8*M* $LiAlCl_4$ in $SOCl_2$)	1690.0	0.143	1000.0	11, 19, 38
Cathode region	1730.0	3.69	957.0	10, 11, 19, 38
Separator region	1250.0	0.173	989.0	10, 11, 38
Core region	1755.0	23.82	1577.0	see Eq. [8]

Model parameters	
Parameter	References
h = 10 W/m^2-K	11, 13, 14
E_{th} = 3.723V	26

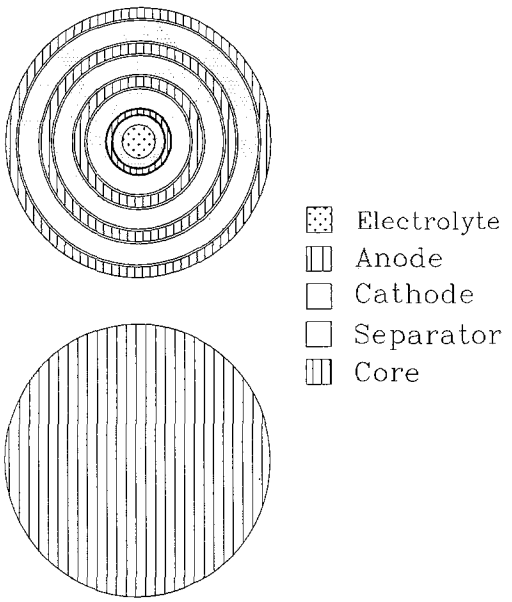

Fig. 4. One-dimensional approximations to the spiral design. The top schematic is the concentric circles approximation and the bottom schematic is the core region approximation.

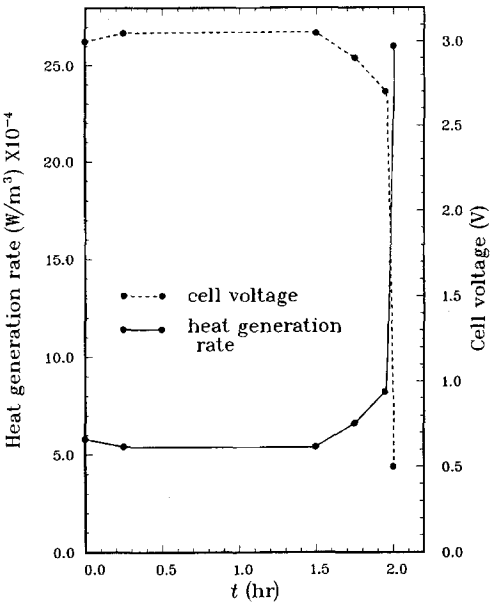

Fig. 6. Heat generation rate and cell voltage for a 4A discharge

state equation set for the core approach is easily solved analytically. Also, these two cases represent two different extremes. The circles case should yield a maximum temperature drop from the center of the cell to the cell exterior, because all heat is forced to flow radially through all cell regions, including the separator region which offers the most resistance to heat flow. The core case should yield a minimum temperature drop from the center of the cell to the exterior, because the thermophysical properties of the core region closely resemble those of the most conductive regions, as shown in Table II. The spiral case, as shown in Fig. 3, should yield temperature profiles somewhere between these two extremes. Heat flow in the radial direction is inhibited by the separator; however, heat can flow out the spiral along the more conductive materials. In the results which follow, the core approximation, the concentric circular regions approximation, and the spiral case are referred to as core, circles, and spiral, respectively.

Comparison of the core, circles, and spiral models.— Figure 5 shows predicted time-temperature profiles for the core, circles, and spiral cases for a 4A discharge. The heat generation rate program, shown in Fig. 6, was calculated using Eq. [5] and the voltage transient shown in Fig. 6. The voltage transient was approximated from experimental results reported in the literature (2, 6, 33). Voltage transients can also be predicted from earlier models (13, 14). It should be noted that there exists a wide range of data for the $Li/SOCl_2$ cell reported in the literature due to differences in the discharge rates, electrode materials, and cell designs investigated (2-6, 25, 33-36). Notice in Fig. 5 that the predicted maximum and minimum temperature dependence on time for the spiral case falls between those of the core and circles cases, as expected. Also note that the core case shows an essentially uniform cell temperature, whereas the circles and spiral cases show about a 2 K temperature drop from the cell interior (T_{max}) to the cell wall (T_{min}). The general shape of the curves are in qualitative agreement with experimental temperature-time curves (6), as shown in Fig. 9, an initial rise in temperature as the electrodes are first polarized, then a plateau is reached where heat generation is about equal to heat transfer away from the cell, then a sharp increase in cell temperature at the very end of the discharge. A comparison of model predictions presented here and experimental results (6) is made below.

The two-dimensional temperature profile for the spiral cell at approximately 1.5h of discharge (corresponding to the dot in Fig. 5) is shown in Fig. 7. The plotted points are the temperatures at each node point of the spiral mesh. The temperature is plotted over the two-dimensional plane defined by x and y shown in Fig. 3. The maximum tem-

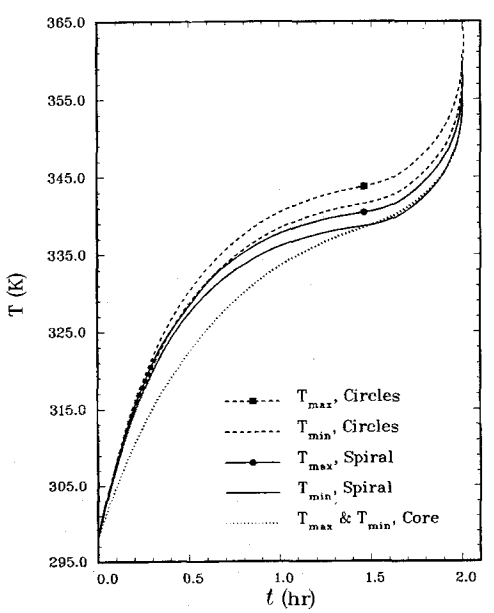

Fig. 5. Temperature-time curves predicted using the core, circles, and spiral models.

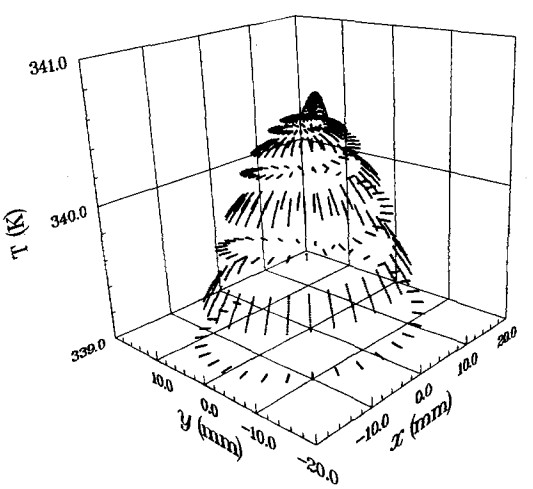

Fig. 7. Predicted temperature profile after 1.5h of discharge

perature is in the electrolyte region located near the center of the cell (see Fig. 3). As shown in Table II, the electrolyte possesses a low thermal conductivity and thus serves to retain heat relative to the other cell components. The temperature drops from this maximum to the minimum temperature located at the outer corner of the spiral, point A in Fig. 3. The largest temperature drops are across the separator and appear as the void spaces between the various levels of the spiral.

Figure 8 shows a comparison of spatial temperature profiles as predicted using the core, circles, and spiral methods. These profiles correspond to approximately 1.5h into the discharge, as shown by the box and dot in Fig. 5. Two profiles are shown for the spiral case, one along vector $\mathbf{y}$ and one along vector $\mathbf{x}_1$ corresponding to the vectors shown in Fig. 3. In order to better compare the profiles, the temperature difference $T - T_{min}$ is plotted on the ordinate. Figure 8 shows that the core approximation does not adequately predict the temperature drop in the spirally wound cell. In this case, the predicted temperature drop is about 2 K according to the spiral model, whereas the core approximation yields only about a 0.2 K drop. Figure 8 also shows that the profiles for the circles approximation and spiral case are in close proximity. The circles approximation is useful because it predicts maximum temperature profiles, as shown in Fig. 5 and 8, and is easily solved in one-dimension using TOPAZ2D.

Several items are noteworthy in the forgoing comparisons between the core, circles, and spiral cases. The spiral model region, shown in Fig. 3, has boundaries different from the core and circles model regions, shown in Fig. 4. The difference is the exposed end of the spiral cell between points A and B in Fig. 3. For the core and circles cases, Eq. [7] is used at the outer boundary. For the spiral, Eq. [7] is used for the outer boundary (clockwise from point A to point B in Fig. 3) and Eq. [6] is used for the end of the spiral cell (counterclockwise from point A to point B in Fig. 3). This use of insulated boundary conditions at the exposed end represents a worst case; in the actual cell, shown in Fig. 1, the lithium electrode is extended and the rest of the spiral end borders electrolyte. For comparison purposes, Eq. [7] was used for all boundaries of the spiral. The relative temperature drop from the cell interior to the exterior remained essentially the same; however, the absolute temperature profile dropped about 1 K. What can be gleaned from this and the forgoing comparisons is that the spiral design aides in cooling down the cell, as opposed to the circles case, because heat can be conducted out the spiral path as well as out the radial direction. This increase reduces the cell temperatures but does not substantially reduce the temperature drop from the center of the cell to the cell wall.

Finally, the effect of different heat generation rate distributions on the temperature profiles was briefly investigated using the spiral model. Four cases were run: 90% of the heat generation contained within the lithium anode and 10% within the cathode, 10% within the anode and 90% within the cathode, 90% within the separator and 10% within the cathode, and 50% within the anode and 50% within the cathode. Each case yielded about a 2 K temperature drop.

Comparison of circles model with experimental results.—The one-dimensional circles model was used to simulate the temperature profiles for an experimental test case reported by Abraham *et al.* (6) for a C-size $Li/SOCl_2$ cell. The component dimensions, cell volume, and other test conditions given in their paper were used in the model; eight wraps were assumed. The heat generation rate program was calculated based on the voltage transients shown in Fig. 7 of their work. The value of the heat transfer coefficient was set to 15 W/m-K, instead of 10 W/m-K as in Table II, in order to match predictions to the experimental data as closely as possible.

The experimental temperature-time curves for the 4A discharge of a catalyzed $Li/SOCl_2$ cell are shown in Fig. 9. The difference in cell temperature from the center of the cell to the can wall is shown to be as much as 13 K. Model predictions, not those shown in Fig. 9, show only about a 3-4 K temperature drop. The model predictions given in Fig. 9 show about an 8 K temperature drop and were obtained by making several changes to the model as described below. Several factors could account for the differences between the model predictions and the experimental measurements. First, this data is for a cell having porous cathodes containing 5 weight percent (w/o) dibenzotetraazaannulene complex of cobalt (Co-TAA). These catalyzed cells exhibit different discharge behavior from uncatalyzed cells (6), and the heat generation rate, as predicted using Eq. [5] and the thermoneutral potential listed in Table II, used in the model may not be appropriate. Assuming that this difference has no effect on model predictions, several other factors may be considered. The heat generation within the cell may not be uniform; it is probable that heat generation is greatest near the center of the cell and diminishes in value when approaching the cell exterior. This can be explained by considering the current density; near the center of the spirally

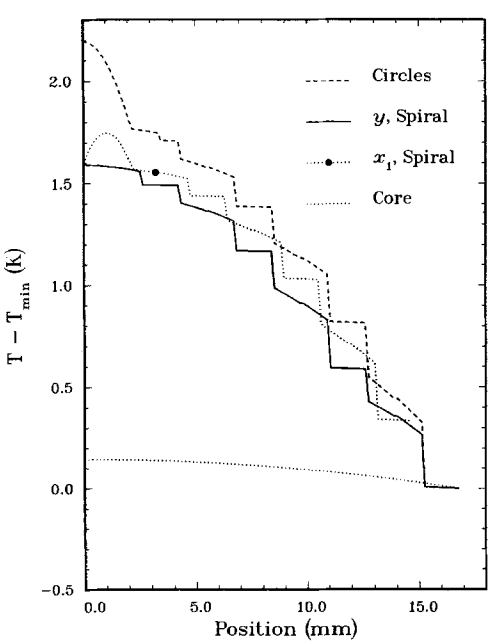

Fig. 8. Radial temperature profiles as predicted using the core, circles, and spiral models.

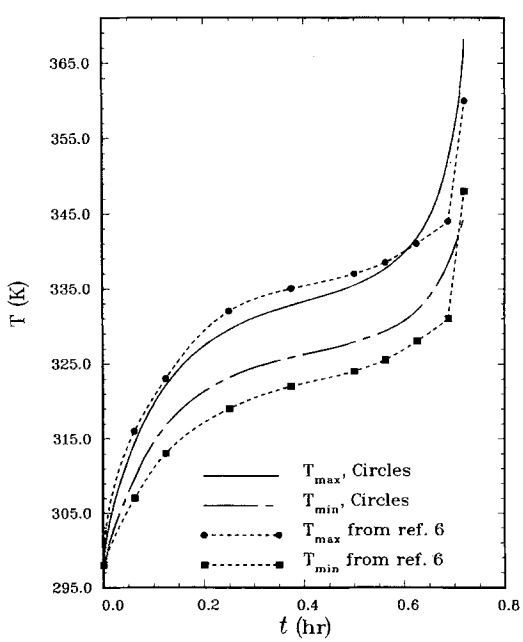

Fig. 9. Comparison of predicted and experimental temperature-time curves for a 4A discharge of a C-size $Li/SOCl_2$ cell.

wound cell there exists less electrode area over which the radially flowing current is distributed than at radii further from the center of the cell. Thus, the electrochemical reaction rate would be greatest at the center, evolving more heat at the center, and would decrease from there to the cell exterior. This argument assumes sufficient resistance in the metallic parts of the electrodes so that there exists an appreciable drop in electrode potential from the inner portion of the electrode spiral to the outer portion. Decreasing thermal conductivities could also explain these large temperature drops. As the cell is discharged, the $SOCl_2$ electrolyte is reduced at the cathode and is sometimes depleted to the point where cell gases fill some of the voids previously occupied by electrolyte (32). To approximate these possibilities, two changes were made to the model. The heat generation rate was set to a maximum value in the first concentric cell (relative value of 4) and was decreased linearly to a minimum value in the eighth concentric cell (relative value 1). The densities, heat capacities, and thermal conductivities of the regions containing electrolyte were changed by assuming that at the end of the discharge only SO_2 remained in the void portions of these regions. These properties were changed linearly throughout the discharge from their starting values, reported in Table II, to their ending values, reported in Table III. The model predictions are superimposed on the experimental data in Fig. 9. Agreement between predictions and experiment has been improved by these changes. Steeper heat generation rate profiles were tried, resulting in larger temperature drops, but the temperature-time relationships did not agree well with the experimental results in Fig. 9. It should be possible to improve the fit of the theoretical predictions to the experimental results by using a parameter estimation technique in conjunction with TOPAZ2D.

These differences between experiment and model indicate several possibilities. Perhaps a more detailed program for the heat generation rate is needed. Other chemical or electrochemical reactions could be occurring, especially at these high rates of discharge, which cause greater heat generation rates; these reactions could be localized. The thermal runaway simulations presented next were run with some of these thoughts in mind. More experimental data, including temperature measurements throughout the cell from center to wall, are needed to analyze thoroughly the temperature profiles in the spirally wound cells and to refine the modeling.

Thermal runaway simulation.—Explosive failures are often associated with localized temperatures above the melting point of Li (2, 3). Therefore, initiation of thermal runaway was simulated by assuming that a hot spot, located near the center of the cell, is formed via a localized exothermic chemical reaction (for example, between Li and sulfur or a sulfur compound) or cell defect. Two simulations were run with the hot spot located at two different points in the cell. For case one, the hot spot was located at the center of the cell in the separator region bordering the cathode and electrolyte. For case two, the hot spot was located in the center of the electrolyte in the middle of the spiral. Case two was also approximated using the one-dimensional circles model for comparison purposes. The hot spot areas were approximately 0.031 and 0.029 mm^2 for case one and two, respectively. The finite element meshes were refined until results were accurate to within 1 K for case one and 3.5 K for case two.

The conditions under which thermal runaway usually occurs include high discharge rates and high temperatures (2, 3-5). Therefore, the inputs to the model included an environmental temperature of 390 K, a uniform initial temperature in the cell of 390 K, and a uniform heat generation rate of 1×10^5 W/cm^3. The hot spot heat generation rate, $\dot{q}'''_d$, was set equal to 5×10^8 W/cm^3. The simulations were run until the minimum temperature in the cell exceeded the melting point of Li (453.6 K). It was assumed that when temperatures exceed the melting point of Li, molten Li bridges the gap between anode and cathode, forming an internal short circuit. Upon forming the short, it was assumed that $\dot{q}'''_d$ would become infinitely large, the temperature would soar, and in a matter of milliseconds the cell would vent or explode (11).

Table III. Thermophysical properties of porous regions assuming that the voids are filled with SO_2 at approximately 20 psig and 60°C.

Material	Density (kg/m^3)	Thermal conductivity (W/m-K)	Specific heat (J/kg-K)	References
SO_2	5.54	0.00816	654.0	39
Cathode region	298.0	3.577	662.0	
Separator region	70.0	0.0783	746.3	

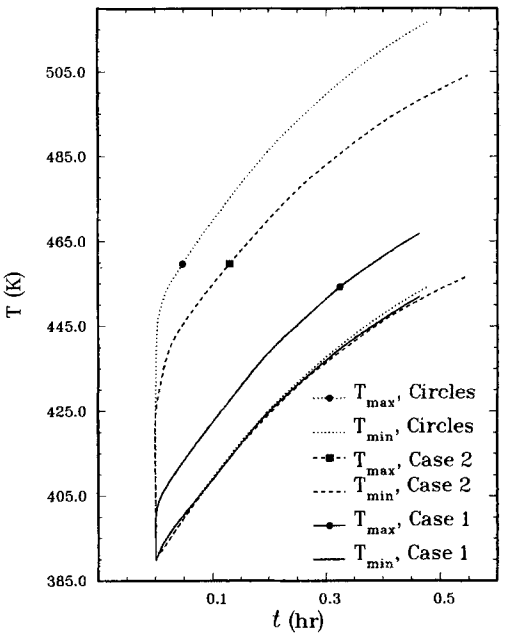

Fig. 10. Temperature-time curves for two thermal runaway cases

Figure 10 shows the maximum and minimum temperature-time curves for case one, case two, and the circles approximation to case two. The maximum temperature increases much more rapidly in case two than in case one. In case two, the hot spot is isolated from the more conductive regions of the cell by the electrolyte. In case one, the hot spot borders the cathode region and the heat is better conducted out the cell via the spiral path. Note that the spiral geometry still improves the heat transfer in case two as is indicated by the higher temperatures predicted using the circles model. A circles approximation to case one, not shown in Fig. 10, using four concentric cells with no electrolyte in the center was run to determine the importance of the radial heat transfer. Still, the maximum tempera-

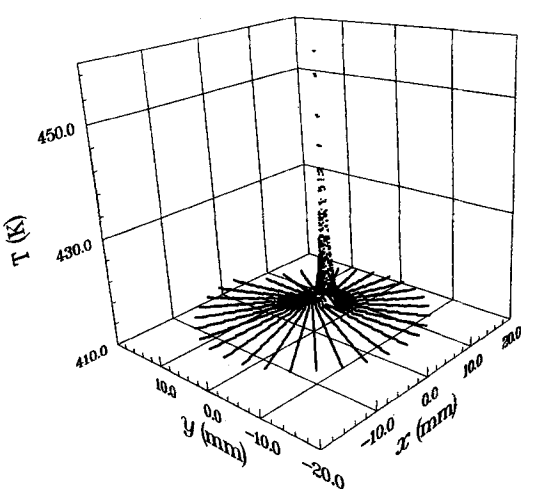

Fig. 11. Temperature profiles in spirally wound Li/$SOCl_2$ cell for thermal runaway case two approximately 470s after hot spot initiation. Internal temperatures exceed the melting point of lithium.

tures predicted were about 5 K higher than those in case one. This result suggests that heat conduction out the spiral path is substantial under this thermal runaway condition.

Figure 11 shows a two-dimensional temperature profile for case two approximately 470s after initiation of the hot spot, corresponding to the box in Fig. 10. A temperature spike is located in the electrolyte region where the hot spot is centered. Note that minimum temperatures exist around most of the cell perimeter except for a portion of the cell located near the end of the spiral (*i.e.*, between points A and B in Fig. 3). This rise in temperature at the spiral end is due to the insulated boundary conditions applied at this boundary. In the actual cell (Fig. 1), the end of the spiral borders electrolyte (or cell gases if the electrolyte has been used up) and one would expect heat flow to be inhibited at this juncture. This result indicates that it is important how the end of the spiral is treated in the actual design. If possible, the end of the spiral should be in close proximity to the case can and void space should be minimized. Researchers (3) have observed that the temperature distribution over the exterior wall of the cell varies, some regions at high temperatures relative to the rest of the exterior surface. Perhaps these high-temperature areas correspond to the location of the spiral end in the cell interior.

Many situations, both normal operation and thermal runaway conditions, can be simulated using the model. These simulations can lead to a better understanding of the thermal behavior of this design as has been achieved here. Indeed, the power of the model lies in the ability to investigate various scenarios simply by changing model inputs. The modeling can also be used as an aid in the interpretation of experimental data, as has been done here.

Conclusions

A two-dimensional thermal model of a spirally wound $Li/SOCl_2$ cell has been developed. The model and two one-dimensional approximations have been used to better understand the thermal behavior of this battery. Comparison of model predictions with experimental data support two contentions. The heat generation rate seems to be greatest at the center of the cell and diminishes toward the exterior of the cell. Also, thermal conductivities seem to decrease as the cell discharges. This could be due to the increasing volume occupied by cell gases as the discharge proceeds. Two thermal runaway situations were investigated using the model, based on the theory that localized hot spots initiate thermal runaway. The effectiveness of the spiral design in conducting heat out of the cell is dependent upon where these hot spots are located in the cell. If hot spots are in contact with those regions of the cell having relatively high thermal conductivities, then the spiral design serves to improve heat dissipation.

The model could be modified to investigate other physical situations. For example, forced convection, radiation, and conduction (via a potting material, *e.g.*) at the cell boundaries could be included in the boundary conditions of the model. Also, the model could be applied to other spirally wound batteries simply by changing model inputs (*e.g.*, thermal conductivities, thermoneutral potential). Improvements to the model might include extending the model to three dimensions using the computer code TOPAZ3D (37), including contact resistances between regions, and adding temperature-dependent thermophysical properties (10).

Acknowledgments

The authors gratefully acknowledge the National Aeronautics and Space Administration for their funding of this work under Grant No. NAG. 9-177. Also, the authors wish to thank Eric Darcy and Bob Bragg at the National Aeronautics and Space Administration for their input to this work, Art Shapiro at the Lawrence Livermore National Laboratory for his help in debugging input files to TOPAZ2D, the professionals at the Jet Propulsion Laboratory for their suggestions for the modeling, and the Cray Research Center, Incorporated, in Houston, Texas for use of their CRAY. Special thanks are given to Dr. David Dealy for providing the Cray computer time and to Bill Eue at the Cray Research Center for his help in converting some of the program code.

Manuscript submitted April 28, 1988; revised manuscript received Dec. 1, 1988.

Texas A&M University assisted in meeting the publication costs of this article.

LIST OF SYMBOLS

$c_{p,k}$	heat capacity of material k, J/kg-K
E	cell voltage, V
E_{oc}	open-circuit voltage of the cell, V
E_{tn}	thermoneutral potential of the cell, V
$\mathbf{F}$	Faraday's constant, 96,487 C/mol of electrons
h	heat transfer coefficient, W/m^2 K
I	total cell current, A
n_x	normal vector in the x direction
n_y	normal vector in the y direction
p_k	property of material k
$\bar{p}$	average property of core region
$\dot{q}'''_j$	heat generation rate due to source j, W/m^3
$\dot{q}'''_p$	heat generated rate due to cell polarization, W/m^3
$\dot{q}'''_s$	heat generated rate due to entropy effects, W/m^3
t	time, s
T	cell temperature, K
T_A	ambient temperature, K
V_{cell}	cell volume, m^3
x	dimension defining two-dimensional plane, m
y	dimension defining two-dimensional plane, m

Greek Symbols

δ_k	thickness of region k, m
ϵ	porosity or void volume fraction
λ_k	thermal conductivity of region k, W/m-K
ρ_k	density of material k, kg/m^3

Subscripts

A	ambient conditions
k	region k
j	source j (either p, s, or d)
oc	open circuit
w	conditions at the wall
x	x dimension
y	y dimension

REFERENCES

1. D. H. Johnson, A. D. Ayers, R. L. Zupancic, V. S. Alberto, and J. C. Bailey, *J. Power Sources*, **12,** 61 (1984).
2. S. Surampudi, G. Halpert, and I. Stein, "Safety Considerations of Lithium-Thionyl Chloride Cells," Jet Propulsion Laboratory publication 86-15 (June 1986).
3. J. B. Trout, "Studies of Performance and Abuse Resistance of Lithium-Bromine Complex Cells for Manned Space Use," NASA internal note JSC-20006, July 1984.
4. N. C. Luksa, "Li-BCX D-Cell Overdischarge," NASA internal note JSC-19262, October 1983.
5. D. Saucier, "Lithium BCX Cell Overdischarge Test," NASA internal note JSC-19548, April 1984.
6. K. M. Abraham, L. Pitts, and W. P. Kilroy, *This Journal*, **132,** 2301 (1985).
7. S. Szpak and H. V. Venkatasetty, *Power Sources 9: Research and Development in Non-Mechanical Electrical Power Sources*, Proceedings of the 13th International Power Sources Symposium held at Brighton, Sept. 1982, J. Thompson, Editor, Academic Press, London, England, 403 (1983).
8. D. Bernardi, E. Pawlikowski, and J. Newman, *This Journal*, **132,** 5 (1985).
9. J. Lee, K. W. Choi, N. P. Yao, and C. C. Christianson, *ibid.*, **133,** 1286 (1986).
10. L. A. Parnell and S. Szpak, *Electrochim. Acta*, **30,** 913 (1985).
11. S. Szpak, C. J. Gabriel, and J. R. Driscoll, *Electrochim. Acta*, **32,** 239 (1987).
12. Y. I. Cho and G. Halpert, *J. Power Sources*, **18,** 109 (1986)
13. T. I. Evans, T. V. Nguyen, and R. E. White, *This Journal*, **136,** 328 (1989).
14. K. C. Tsaur and R. Pollard, *ibid.*, **131,** 975 (1984).
15. K. C. Tsaur and R. Pollard, *ibid.*, **131,** 984 (1984).
16. K. C. Tsaur, Ph.D. Dissertation, University of Houston, Houston, TX (1984).

17. K. C. Tsaur and R. Pollard, *This Journal*, **133**, 2296 (1986).
18. Y. I. Cho and G. Halpert, in "Proceedings of the 32nd International Power Sources Symposium," Cherry Hill, NJ, June 9-12, 1986, The Electrochemical Society, Inc., p. 547 (1986).
19. Y. I. Cho, *This Journal*, **134**, 771 (1987).
20. J. Newman and W. Tiedemann, *AIChE. J.*, **21**, 25 (1975).
21. J. A. Trainham, Ph.D. Dissertation, University of California, Berkeley, CA (1979).
22. K. Nisancioglu, M.S. Thesis, University of California, Berkeley, CA (1970).
23. J. Newman, D. Bennion, and C. W. Tobias, *Ber. Bunsenges, Phys. Chem.*, **69**, 608 (1965).
24. J. S. Newman, "Electrochemical Systems," Prentice Hall, Inc., Englewood Cliffs, NJ (1973).
25. K. A. Klinedinst, *This Journal*, **132**, 2044 (1985).
26. N. A. Godshall and J. R. Driscoll, *ibid.*, **131**, 2221 (1984).
27. L. D. Hansen and H. Frank, *ibid.*, **134**, 1 (1987).
28. L. Lapidus and G. F. Pinder, "Numerical Solution of Partial Differential Equations in Science and Engineering," John Wiley & Sons, Inc., New York (1982).
29. A. B. Shapiro, "TOPAZ2D—A Two-Dimensional Finite Element Code for Heat Transfer Analysis, Electrostatic, and Magnetostatic Problems," Lawrence Livermore National Laboratory, UCID-20824 (July 1986).
30. J. O. Hallquist, "MAZE—An Input Generator for DYNA2D and NIKE2D," Lawrence Livermore National Laboratory, UCID-19029, Rev. 2 (June 1983).
31. Wilson-Greatbatch, Personal communications.
32. B. Bragg and E. Darcy, NASA, Personal communications.
33. W. K. Behl, J. A. Christopulos, M. Ramirez, and S. Gilman, *This Journal*, **120**, 1619 (1973).
34. J. J. Auborn, K. W. French, S. I. Lieberman, V. K. Shah, and A. Heller, *ibid.*, **120**, 1613 (1973).
35. K. A. Klinedinst and M. J. Domeniconi, *ibid.*, **127**, 539 (1980).
36. A. N. Dey, *ibid.*, **126**, 2052 (1979).
37. A. B. Shapiro, "TOPAZ3D—A Three-Dimensional Finite Element Heat Transfer Code," Lawrence Livermore National Laboratory, UCID-20484 (August 1985).
38. G. Halpert, Jet Propulsion Laboratory, Personal communications.
39. J. A. Dean, "Lange's Handbook of Chemistry," 13th ed., McGraw Hill Book Co., Inc., New York (1985).

Stabilization of Metal-Metal Oxide Surfaces Using Electroactive Polymer Films

Zhi Deng, William H. Smyrl,* and Henry S. White

Corrosion Research Center, Dept. of Chemical Engineering and Materials Science, University of Minnesota, Minneapolis, Minnesota 55455

ABSTRACT

Charge coupling of the catalyzed reduction of O_2 on platinized poly(3-methylthiophene) [P(3-MT)] films to the anodic dissolution of Ti is reported. Specifically, the redox polymer with Pt catalyst is used in these studies to mediate electrons generated by Ti dissolution and consumed by O_2 reduction. Due to the large redox polymer capacity (>55 F/cm^3) of P(3-MT), these reactions occur at a stable potential approximately equal to the reversible oxidation potential of the polymer. Data presented support the conclusion that O_2 reduction on the polymer film can replenish polymer charge consumed by metal dissolution, thereby stabilizing the potential of Ti within the passive potential range and minimizing the rate of metal dissolution. O_2 reduction on P(3-MT)/Pt is sufficiently fast to poise the potential of Ti at 0.55V *vs.* SCE for *p*H $\approx$ 3.2 and for metal-to-polymer geometrical area ratios (A_{Ti}/A_{PMT}) $\leq$ 10. These results suggest possible applications of redox polymers as porous cathodes for metal stabilization.

The formation of thin oxide films stabilizes many metals against attack in aggressive environments (1). At steady state, the rate of metal dissolution is suppressed by these oxide films to very low rates, a result which extends the life of the protected metal by orders of magnitude in some cases. Factors such as the chemical and physical properties of the oxide, solution composition (*e.g.*, solution *p*H or the concentration of complexing species), and fluid convection can alter and often diminish the range of protection of oxide films. In addition, because the rate of metal dissolution is generally very low in the passivated state, the potential of free standing specimens is generally unpoised and prone to shifts toward negative potentials (in reducing environments) and positive potentials (in oxidizing environments) where metal dissolution occurs at a more rapid rate (see Fig. 1).

In this paper, we describe a general strategy using redox polymer coatings to stabilize the potential well within the passive region where the metal is covered with an oxide film. Scheme I (Fig. 2a) shows the components of this strategy, where a metal is coated with a thin and porous electroactive polymer film. The role of the polymer is to poise the potential of the oxide-covered metal at an intermediate value between the active and the transpassive potential regions. Thin films of conductive polymers such as poly(3-methylthiophene) or redox polymers such as poly(vinylferrocene), can be partially and reversibly oxidized on inert substrates (*e.g.*, glassy carbon), establishing a well-defined electrode potential that remains constant in the absence of redox reactions that may discharge the polymer to its original neutral state. The potential of a partially oxidized P(3-MT) film, for instance, will drift toward more negative values as the film is chemically reduced. The length of time that the potential is maintained at a particular level is determined by the total charge stored in the film and the rate of (discharge) reactions. Coating an oxidized film of P(3-MT) on Ti/TiO_2 is shown below to control the potential of the metal in the passive range. However, the anodic dissolution current of the passive surface must be compensated in order to stabilize the system. The small but finite anodic current to the passive surface at steady state is determined by the solubility of the oxide in solution. Coupling the passive surface to the oxidized polymer film leads to an irreversible galvanic current and discharge of the polymer according to Eq. [1]

$$(1/n)\mathrm{Ti} + (1/m)\mathrm{P(3\text{-}MT)}^{+m} = (1/n)\mathrm{Ti}^{+n} + (1/m)\mathrm{P(3\text{-}MT)}^{0} \quad [1]$$

The conclusion here is that the polymer film alone will not stabilize the passive surface at steady state, and a second reaction must be used to compensate the anodic dissolution current. In the results to be described below, the polymer film also serves as the site for the second reaction, which is the cathodic reduction of oxygen dissolved in the electrolyte solution (Scheme II in Fig. 2b).

Redox active polymer films such as P(3-MT) are highly permeable and do not offer significant protection as transport barriers. This is advantageous since the dissolution

* Electrochemical Society Active Member.